circuitry. The realized FBAR duplexer for CDMA PCS applications has compatible performance characteristics to the conventional ceramic components. However, the fabricated FBAR duplexer is much smaller size and volume than the ceramic one. The demonstrated FBAR filter and duplexer are also promising for integrated and miniaturized filter banks, RF FEM (Front-End Module), and RF transceiver module.

ACKNOWLEDGMENTS

This research was partially supported by Korea Ministry of Science and Technology under the 21st Frontier Intelligent Microsystem Development Project, University Information Technology Research Center (ITRC) supported by the Ministry of Information and Communication of Korea (2006), and internal research fund of Kwangwoon University in Korea.

REFERENCES

1. REMEC Wireless, Ceramic Filters and Duplexers for Base Station and Microcell Applications, Microwave J 39 (1996), 170–172.
2. M. Hikita, N. Shibagaki, T. Akagi, and K. Sakiyama, Design methodology and synthesis techniques for ladder-type SAW resonator coupled filters, IEEE Ultrasonics Sym (1993), 15–24
3. R.S. Naik, et al., Electromechanical coupling constant extraction of thinfilm piezoelectric materials using a bulk acoustic wave resonator, IEEE Trans Utrasonics Ferro Freq Control 45 (1998), 257–263.
4. K.M. Lakin, J.S. Wang, and A.R. Landin, Aluminum nitride thin film and composite bulk wave resonators, In Proceeding of 36th Annual Frequency Control Symposium, 1982, 517–524.
5. J.Y. Park, H.M. Lee, H.C. Lee, K.H. Lee, Y.J. Ko, and J.U. Bu, Comparison of micromachined FBAR band pass filters with different structural geometry, IEEE MTT-S Dig (2003) 2005–2008.

NEW 0.18-μm CMOS PULSE GENERATOR FOR IMPULSE RADIO ULTRA-WIDEBAND COMMUNICATION SYSTEMS

Tung-Yuan Tzou and Fu-Chiarng Chen
Department of Communication Engineering, National Chiao Tung University, Hsinchu 300, Taiwan

Received 26 June 2006

ABSTRACT: *This article presents a new circuit to generate a higher-order derivative Gaussian pulse for the impulse radio ultra-wideband (IR-UWB) communication systems. This IR-UWB pulse generator is designed and measured with the TSMC 0.18-μm CMOS process. The circuit is able to generate a symmetrical and low-ringing pulse in a frequency band from 3.1 to 10.6 GHz. Our work shows that the pulse generator's output pulse width is 500 ps with an amplitude of 40 mV (peak to peak). The measurement results validate our design and the circuit functionality.* © 2006 Wiley Periodicals, Inc. Microwave Opt Technol Lett 49: 342–345, 2007; Published online in Wiley InterScience (www.interscience.wiley.com). DOI 10.1002/mop.22132

Key words: *ultra-wideband; impulse radio; pulse generator; CMOS*

1. INTRODUCTION

The Federal Communications Commission (FCC) has defined ultra-wideband (UWB) as a fractional bandwidth equal to or greater than 20%, or the bandwidth of the transmitted signal is more than 500 MHz [1]. The UWB technologies have been successfully applied in sensing radar, highly-accurate location positioning, and military communication. Impulse radio (IR) is one of the promising applications of UWB technology. It is a carrierless system that is different from other RF systems using a narrowband carrier. IR-UWB wireless communication utilizes short pulse signals to transmit data over a very wide spectrum of frequency bands for short-range, high date-rate applications. The main advantage of IR-UWB systems is that their architecture is of low complexity and low power [2, 3]. However, the signal bandwidth of the IR-UWB signal may overlap with those of many existing narrowband systems (such as the GPS systems operate around 1.5 GHz). Thus, the FCC has set a spectral mask for the usage of the UWB transmission signal. The specified spectral mask induces design challenge to circuit and system designers [4].

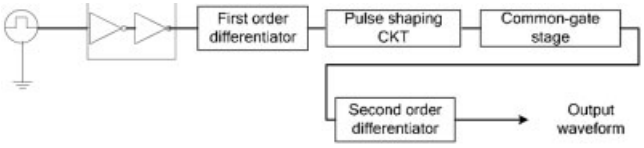

Figure 1 Block diagram of our proposed UWB pulse generator

The pulse generator, a critical part of the IR-UWB transmitter, generates the transmitted waveform which must satisfy the frequency mask. Recently, creative methods have been proposed to implement the pulse generator. Up to now, several articles are presented to generate the Gaussian monocycles or Scholtz's monocycles [5–8]. However, those pulses do not satisfy the FCC spectrum mask and need filtering in order to meet the regulation. The higher-order derivative Gaussian pulse, with hundreds of picoseconds duration, have been found to use adequately in UWB indoor system [9]. Another advantage of the higher-order derivative Gaussian pulse is transmitted without any filtering, and this will decrease the complexity of the architecture without degrading the system performance.

In this article, a new pulse generator is designed and fabricated using the TSMC 0.18-μm CMOS technology for IR-UWB applications. Our work shows that the output pulse width is 500 ps with an amplitude of 40 mV (peak to peak). The circuit is able to generate a symmetrical and low-ringing pulse in a frequency band from 3.1 to 10.6 GHz. In the first part of our article, we describe each block of the circuit and analyze the design principles. The second part is dedicated to the simulation and measurement results. Finally, a short conclusion is discussed.

2. OPERATING PRINCIPLE AND ANALYSIS

2.1. Circuit Description

The functional block diagram of the pulse generator is shown in Figure 1. In the input stage, the oscillator determines the input square signal that has 2 V a and pulse repetition frequency of 100 MHz (up to 500 MHz). Then the signal passing through a simple

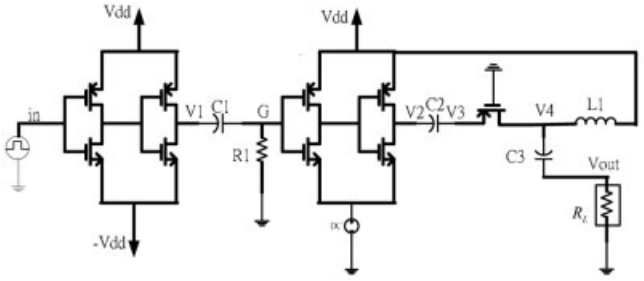

Figure 2 Schematic of the new pulse generator

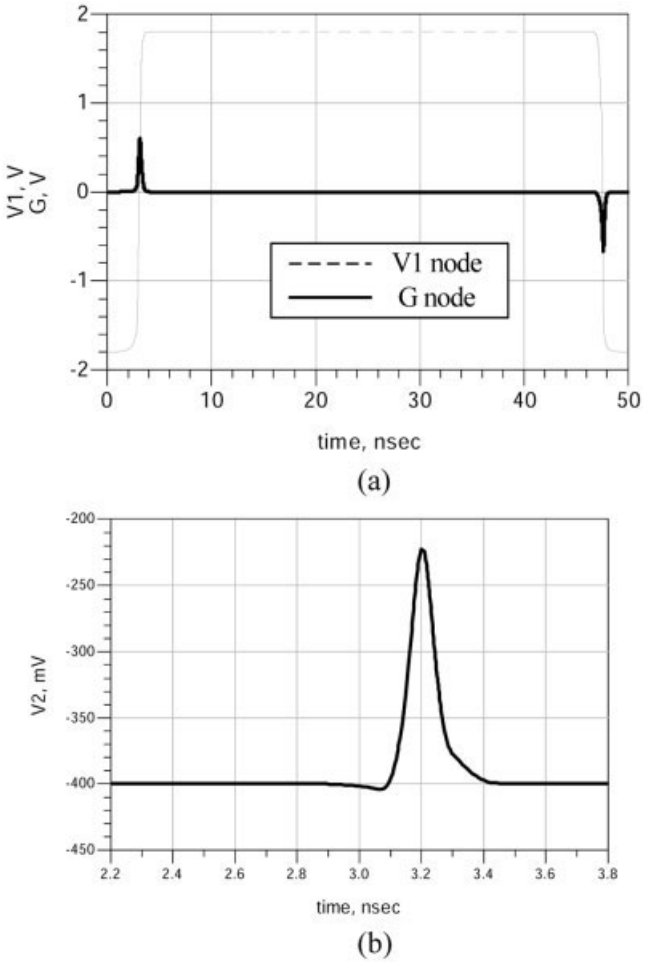

Figure 3 (a) Waveform of the approximate Gaussian pulse, (b) Waveform after the pulse shaping circuit

RC differentiator will produce an approximate Gaussian pulse at the rising edge of the square wave. To shrink the pulse from nanosecond to picosecond level duration, several inverters are adopted to perform the function of pulse shaping. We employ a PMOS transistor as a common-gate amplifier acting as a differentiator. Then the monocycle pulse can be obtained by taking the derivative of the previous Gaussian pulse. Finally, we utilize the second-order RLC differentiator to differentiate the impulse to become a higher-order derivative Gaussian pulse in the output stage.

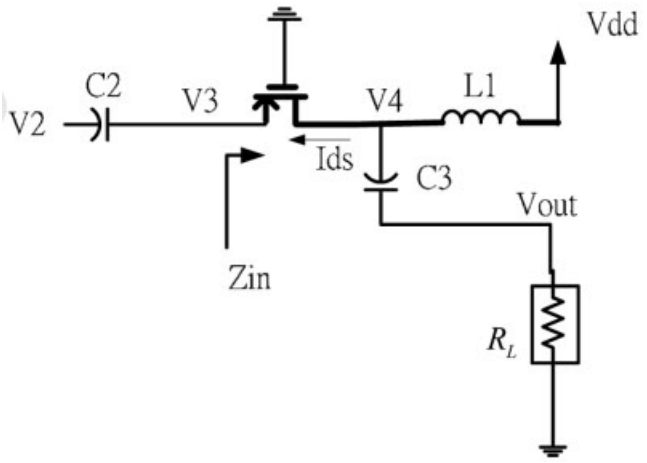

Figure 4 Schematic of the common-gate stage and second-order differentiator

2.2. *Production of the Approximate Gaussian Pulse*

Figure 2 shows the schematic of our new pulse generator. Because the switching speed of the inverters is fast in the 0.18-μm CMOS technology, the two inverters after the input oscillator will increase the rise time and the fall time of the square wave. This results in an edge signal (at V1 node) which serves to drive the first-order

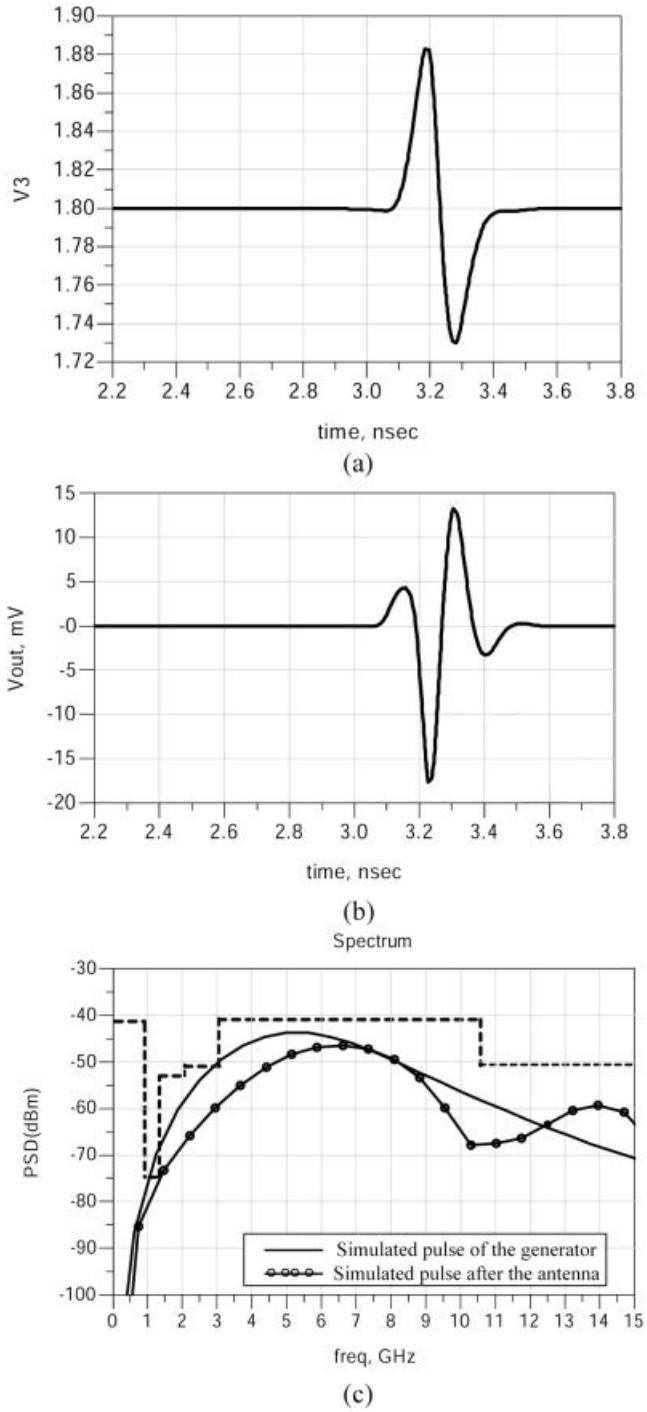

Figure 5 (a) Waveform of the monocycle pulse, (b) Output waveform of the proposed pulse generator, (c) Power spectrum of the output waveform

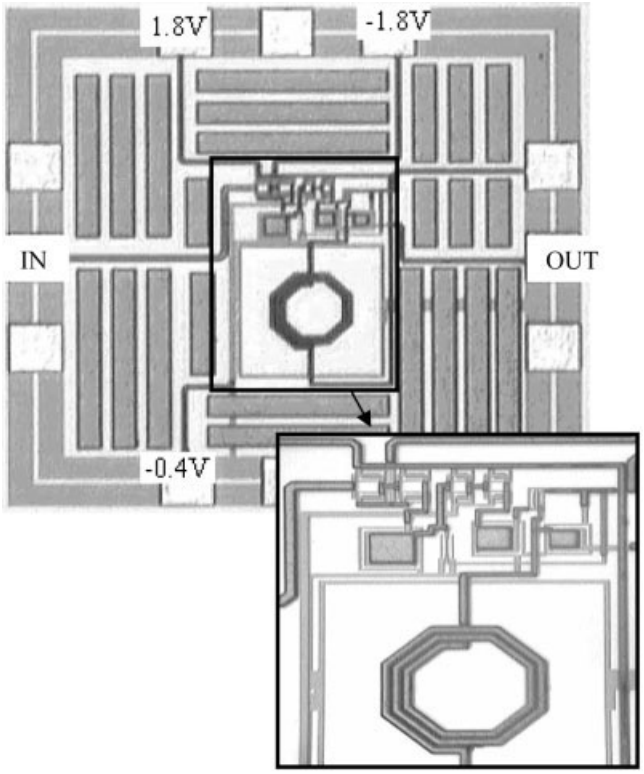

Figure 6 Chip photograph

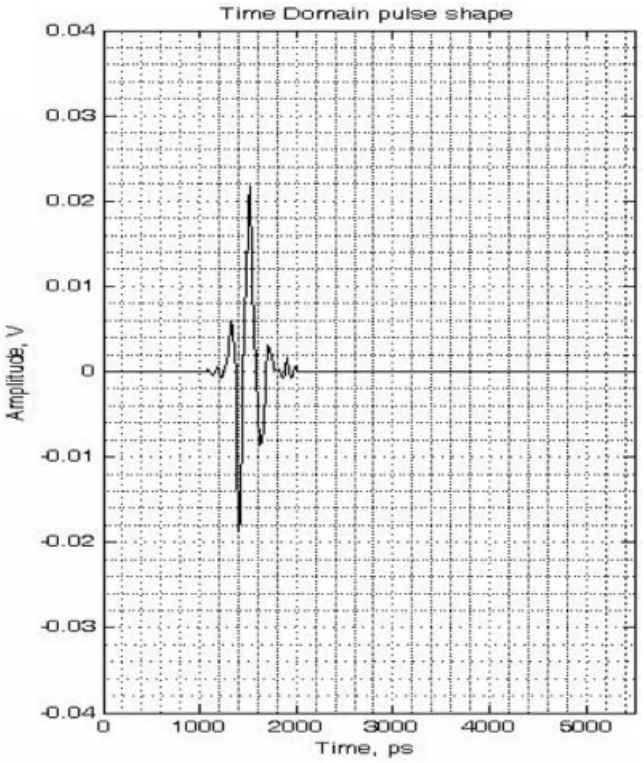

Figure 7 Measured output waveform of the pulse generator

differentiator (C1 and R1). At node *G*, we can obtain approximate Gaussian pulses at the rising and falling edge, respectively. These pulses have durations of 2 ns and amplitudes of 600 mV as shown in Figure 3(a). We employ a couple of inverters as a pulse shaping circuit. It only preserves the positive part (0–600 mV) of the prior Gaussian pulses whose amplitudes are greater than the threshold voltage. By controlling the DC biasing voltage at the source of the NMOS transistors, we can obtain a narrow pulse width of 300 ps, approximately. The simulation result is given in Figure 3(b).

2.3. Output Stage Analysis

There are two reasons why we chose a PMOS transistor as a common-gate stage architecture. First, it provides an isolation to prevent coupling between the capacitor C2 and the second-order RLC differentiator at the next stage. Second, the input impedance of a common-gate stage is relatively low only if the load impedance connected to the drain is small [10]. Figure 4 shows the schematic of the common-gate stage and second-order differentiator used in the design. On the basis of the previous discussion, we can design the input impedance seen at the source (Zin) and the capacitor C2 acting as a simple RC differentiator. Then the so-called monocycle pulse can be obtained by taking the derivative of the previous Gaussian pulse. As shown in Figure 5(a), the resulting pulse width is almost the same as the one before the differentiation. The second-order derivation circuit is composed of L1, C3, and R_L. The output voltage (V_{out}) is a second derivative of the drain current. Figure 5(b) shows the output voltage on 50 Ω load. Figure 5(c) shows the power spectrum density (PSD) of the simulated pulse (solid line) and the simulated pulse after transmission by the UWB antenna (circle type line). The simulation results show that the output pulse width is 400 ps and the pulse amplitude is 43 mV (peak to peak), with more than 7 GHz bandwidth. It is known that the antenna acts as a differentiator. If an UWB antenna has enough bandwidth to pass the signal from the proposed pulse generator, the transmitted pulse can be approximated as the first derivative of the generator's output pulse. Therefore, the output waveform is a higher-order derivative Gaussian pulse and the spectrum is located inside the mask given by FCC after the pulse is transmitted by the antenna as shown in Figure 5(c).

3. FABRICATION AND MEASUREMENT

The proposed UWB pulse generator circuit is implemented using the TSMC 0.18-μm CMOS process. The chip photograph is shown in Figure 6. The whole chip size is 0.84 mm by 0.82 mm and the operating voltage is 1.8 V. The core chip is only 0.23 mm by 0.34 mm and the other area is filled with dummy according to the minimum distance between the pads.

The measurement uses a 50-MHz square wave as the input signal. The I/O matching is designed to perform the measurement onto a 50 Ω load. The measured results are illustrated in Figure 7 and the developed pulse generator performance data is given in Table 1. It has a pulse duration of 500 ps and a pulse amplitude of 40 mV (peak-to-peak). Figure 8 shows the PSD of the measured pulse (solid line) and the PSD of the measured pulse after numer-

TABLE 1 Pulse Generator Performance Data

Process technology	TSMC 0.18-μm CMOS
Carrier frequency	No carrier
Signal bandwidth	3–10 GHz
Pulse repetition rate	Up to 500 MHz
Power consumption	18.33 mW
Pulse width	500 ps
Pulse amplitude	40 mV
Circuit size	0.68 mm^2 (excluding pad)
Application	UWB indoor system

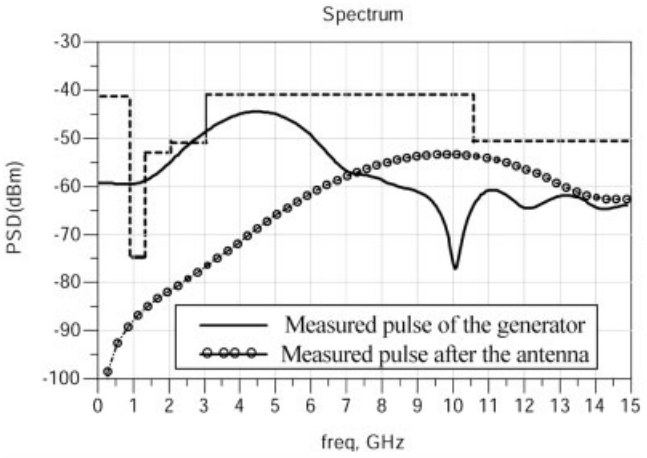

Figure 8 PSD of the measured pulse from the pulse generator (solid line) and the PSD of the pulse after numerically differentiated by a UWB antenna (circle type line)

ically differentiated by a UWB antenna (circle type line). We can find that the PSD of the measured pulse after differentiated by the antenna is under the FCC spectral mask.

4. CONCLUSION

We have designed, fabricated and tested the proposed pulse generator. The complete circuit is designed and fabricated in a standard TSMC 0.18-μm CMOS technology. Our proposed pulse generator has many advantages including a good symmetry, low-ringing, and a wide bandwidth characteristics. The output pulse approximates a higher-order derivative Gaussian pulse with a pulse duration of 500 ps and a 40 mV amplitude. The power consumption of the pulse generator is about 18 mW.

ACKNOWLEDGMENTS

This research was supported in part by a grant of making chips from National Chip Implementation Center (CIC), Taiwan.

REFERENCES

1. IEEE 802.15 WPAN high rate alternative PHY task group 3a (TG3a). Available at http://www.ieee802.org/15/pub/TG3a.html.
2. M.Z. Win and R.A. Scholtz, Impulse radio: How it works, IEEE Commun Lett 2 (1998), 36–38.
3. S. Roy, J.R. Foerster, V.S. Somayazulu, and D.G. Leeper, Ultrawideband radio design: The promise of high-speed, short-range wireless connectivity, Proc IEEE 92 (2004), 295–311.
4. Federal Communications Commission, Revision of part I5 of the commission's rules regarding ultra-wideband transmission, ET Docket 98–153, Federal Communications Commission, April, 2002.
5. J. Han and C. Nguyen, A new ultra-wideband, ultra-short monocycle pulse generator with reduced ringing, IEEE Microwave Wireless Compon Lett 12 (2002), 206–208.
6. H. Kim, D. Park, and Y. Joo, Design of CMOS Scholtz's monocycle pulse generator, In Proceeding of the IEEE Conference on UWB Systems and Technologies, 2003.
7. S. Bagga, W.A. Serdijn, and J.R. Long, A PPM Gaussian monocycle transmitter for ultra-wideband communications, In Proceeding of the IEEE Conference on UWB Systems and Technology, 2004.
8. A. Azakkour, M Regis, F Pourchet, G. Alquie, A new integrated monocycle genarator and transmitter for ultra-wideband communications, In Proceeding of the IEEE Radio Frequency Integrated Circuits Symposium, 2005.
9. H. Sheng, P. Orlik, A.M. Haimovich, L.J. Cimini, and J. Zhang, On the spectral and power requirements for ultra-wideband transmission, In Proceedings of IEEE International Conference on Communications, Anchorage, AL, March, 2003, vol. 1, pp. 738–742.
10. B. Razavi, Design of analog CMOS integrated circuits, McGrawHill, New York, 2002.

A COMPACT DUAL-BAND DUAL-POLARIZED PATCH ANTENNA FOR 1800/5800 MHz CELLULAR/WLAN SYSTEMS

Don-Yen Lai and Fu-Chiarng Chen
Department of Communication Engineering, National Chiao Tung University, Hsinchu 300, Taiwan

Received 2 July 2006

ABSTRACT: *In this paper, we present a compact dual-band dual-polarized aperture-coupled patch antenna for 1800/5800 MHz DCS/WLAN applications. With properly designed feeding network and patch dimensions, the antenna can provide a pair of orthogonal linear polarization states for dual bands operations.* © 2006 Wiley Periodicals, Inc. Microwave Opt Technol Lett 49: 345–349, 2007; Published online in Wiley InterScience (www.interscience.wiley.com). DOI 10.1002/mop.22129

Key words: *polarization-diversity; dual-polarization; aperture-coupled patch antenna; dual-band antennas; diplexing feeding network*

1. INTRODUCTION

Dual-band and dual-polarized antenna is attractive in wireless communication systems due to its several advantages. First, the dual frequency functionality allows us to integrate different systems into one single device. Second, polarization diversity can be utilized to realize frequency reuse due to its useful polarization modulation scheme. This property has been applied in active read/write microwave tagging systems [1]. Third, polarization diversity is effective in avoiding the fading loss caused by multipath effects [2]. There are many ways to implement polarization diversity antennas. Aperture-coupled patch antenna with dual slots which are fed by a dual port-feeding network is introduced recently [3, 4]. In Ref. 3, a patch antenna uses dual orthogonal H-slots to excite a pair of orthogonal modes in the patch. In Ref. 4, a ring patch antenna with apertures which are fed by dual ports feeding operate at 1.8 GHz is presented. In Ref. 5, there are three methods to make dual frequency resonance possible: orthogonal-mode method, multi-patch method, and reactively loaded method. In this work, we focus on integrating two different resonance frequencies patches into an antenna system for 1800/5800 MHz wireless applications. For multipatches designing, printing more resonant patches on the same substrate is low cost and lightweight than multilayer stacked patches [5]. In Ref. 6, the compact microstrip patch antenna for GPS and DCS application is proposed. The antenna system consists of a truncated square patch antenna and an annular ring patch. The former offers a right hand circular polarization at 1575 MHz, which is suitable for GPS application. The later operates at the TM_{21} mode at 1800 MHz, which is appropriate for DCS application. In Ref. 7, the authors present a compact dual-band dual-polarized patch antenna for 900/1800 MHz cellular systems. An elaborate diplexer for 900/1800 MHz is